

**ON IDENTIFICATION OF DAMAGE IN STRUCTURES  
VIA WAVE TRAVEL TIMES**

S.S. IVANOVIC<sup>1)</sup>, M.D. TRIFUNAC<sup>2)</sup> and M.I. TODOROVSKA<sup>2)</sup>

*<sup>1)</sup>University of Monte Negro, Department of Civil Engineering*

*Cetinjski Put BB, Podgorica 81000, Monte Negro, Yugoslavia*

*<sup>2)</sup>University of Southern California, Department of Civil Engineering*

*Los Angeles, CA 90089-2531, U.S.A.*

Key Words: damage identification, wave propagation, travel time.

**ABSTRACT**

The traditional identification methods for detection of damage and for health monitoring of structures are based on detection of changes in the system natural frequencies. These changes tend to be small in the early stages of damage, and therefore may be difficult to quantify, even from accurately processed recorded motions. Other difficulties arise from the nonuniqueness in the model representation. Unless the model accounts for the soil-structure interaction, and it has been carefully validated and calibrated, it is very difficult to identify the true causes and sources of observed nonlinearities in the response. In this paper, it is suggested that the formation of damaged zones in structures could be monitored (identified) via the delays in travel times of seismic waves through these zones. This approach needs further development and testing. A preliminary analysis presented in this paper (of a building damaged by the 1994 Northridge, California, earthquake) shows that this method (1) can lead to detectable changes in the travel times of the waves passing through the areas known to have experienced damage, and (2) in its simplest form does not to require detailed modeling or analysis of soil-structure interaction.

**1. INTRODUCTION**

One of the purposes for testing full scale structures, before during and after earthquakes, is to detect damages caused by severe earthquake shaking [3, 15]. In ideal setting, the measurements should identify the location, evolution and the extent of damage. For example, the recorded data would show the time history of reduction of stiffness in the damaged member(s), and would identify the damaged member(s). Minor damage, which weakens the structural members but does not alter the form of their participation in the overall stiffness matrix, is expected to be reflected only in changes of the corresponding terms of the system stiffness matrix, and this will result in changes of the corresponding mode shapes and natural periods of vibration [19]. Consequently, a partially damaged member would reduce the overall stiffness of the system, and would cause the natural periods of vibration to lengthen. A simple approach to structural health monitoring has been to measure these changes in the natural periods (usually the first period,  $T_1$ ) before and after strong shaking [5]. However, there are at least two problems with this approach. The first problem is that such period changes are usually small, and therefore are difficult to measure accurately [7]. The second problem is that the apparent system period,  $T$ , which is the quantity usually measured, depends also on the properties of the foundation soil, i.e.

$$T^2 = T_1^2 + T_r^2 + T_h^2 \quad (1)$$

where  $T_1$ —first fixed-base building period,  $T_r$ —period of the building rocking as a rigid body on flexible soil, and  $T_h$ —period of the building translating horizontally as a rigid body on flexible soil. The apparent system period,  $T$ , can and often does change appreciably during strong shaking, by factors which can approach two [20]. These changes are caused mainly by nonlinear response of the foundation soils, and appear to be self-healing, probably due to dynamic settlement and compaction during aftershocks and small earthquakes [5, 17]. To detect changes in  $T_1$  only, special purpose instrumentation must be installed in structures. With the currently available instrumentation in various buildings in California, one can evaluate changes in  $T$ , but separate contributions from  $T_r$ ,  $T_h$  and  $T_1$  cannot be detected [6].

For periods shorter than  $T$  (this corresponds to short wave lengths and to higher modes of building vibration), the soil-structure interaction effects become more complex and must be analyzed by wave propagation methods [12, 13]. In principle this higher complexity may offer good resolution for the purposes of identification of the soil-structure parameters, but this depends also on our ability to model the system realistically and calls for far more detailed full scale tests. Therefore most studies consider measured data only in the vicinity of  $T$ .

To illustrate the order of magnitude of the changes in  $T_1$ , we consider the model shown in Fig. 1. Let us assume that this model deforms in shear only, and let the period of the first mode of vibration be equal to  $T_1$ . Since the mode-shapes represent interference patterns of shear waves propagating up and down the structure [9, 11], it can be shown that the period  $T_1$  is proportional to the travel time  $H/b$  ( $T_1 = 4H/b$  and  $b =$  shear-wave velocity in this structure), before any damage has occurred. After strong shaking, suppose that some columns have been damaged at a particular floor. Let the “length” of this damaged zone be  $h_d$ , and the reduced velocity of shear waves within this damaged zone,  $b_d$ . Then the period of the first mode will be proportional to  $T_d \sim (H-h_d) / b + h_d / b_d$ , and the

percentage increase in  $T_d$ , relative to  $T_1$ , will be  $p = \frac{100h_d}{H} \left( \frac{b}{b_d} - 1 \right)$ . For example, for  $H = 20$  m,  $h_d = 2$  m,  $b = 100$  m/s and  $b_d = 50$  m/s,  $p = \frac{100 \times 2}{20} \left( \frac{100}{50} - 1 \right) = 10$  percent.

In the following, we explore whether simple measurements of wave velocity in structures during strong shaking can be carried out, and whether the location of the observed changes will coincide with the areas of observed damage. For this purpose, we analyze strong motion recordings in a 7-storey reinforced concrete hotel building in Van Nuys, California, severely damaged by the 1994 Northridge earthquake. We show that this task appears to be feasible, and suggest that accurate digitization of accelerograms recorded in buildings is essential, before this type of analysis can be further developed and refined.

## 2. METHODOLOGY

Let it be assumed that recordings of strong motion are available at two adjacent floors, and that it is possible to measure the velocity of shear waves propagating in the structure. Before damage has occurred, the travel time between two adjacent floors,  $i$  and  $j$ , would be

$$t_{i,j} = H^*/b \quad (2)$$

and after damage has occurred

$$t_{i,j}^d = (H^* - h_d) / b + h_d / b_d, \quad (3)$$

where  $H^* = H/N$ ,  $N$  = the number of stories (in our example,  $N = 7$ ), and  $H^*$  = story height. The percent change from  $t_{i,j}$  to  $t_{i,j}^d$  is then  $p = \frac{100h_d}{H^*} \left( \frac{b}{b_d} - 1 \right)$ . For  $h_d = 2$  m,  $b_d = 0.5b$ , and  $H^* = 20/7$  m,  $p = \frac{100 \times 2 \times 7}{20} \left( \frac{1}{5.0} - 1 \right) = 70$  percent. Note that this is  $N$  times larger than the percent change in  $T_1$ , because the observation “length” has been reduced  $N$  times.

A typical value of  $H^*$  is 3 m and of  $b$  is 100 m/sec; then  $t_{i,j} \sim 0.03$  sec. Old data processing of strong motion acceleration provided equally spaced data at 50 points/s. Since the early 1990's, most data is processed with time step  $\Delta t = 0.01$  s or 100 points/s. Clearly, to detect time delays of the order of 0.03, the accuracy of origin time and the accuracy of the time coordinates in digitized and processed data must be better than 0.03 s.

### 3. RESULTS

#### 3.1 Building Description

The building we study is a 7-story reinforced concrete hotel building in Van Nuys, central San Fernando Valley, California (Fig. 2). It was designed in 1965 [1] and constructed in 1966. Its plan dimensions are approximately 63 by 160 feet (Fig. 3a; 1 foot=0.3048 m). The typical framing consists of columns spaced at 20 foot centers in the transverse direction (Fig. 3b) and 19 foot centers in the longitudinal direction. Spandrel beams surround the perimeter of the structure. Lateral forces in each direction are resisted by interior column-slab frames and exterior column spandrel beam frames. Due to the stiffness added by the spandrel beams, the exterior frames are approximately twice as stiff as the interior frames. With the exception of some light framing members supporting the stairway and elevator openings, the structure is essentially symmetric. The participation in the response of the nonstructural brick filler walls and some exterior cement plaster could cause some asymmetry for lateral motion in the longitudinal direction, expected to be minor.

The first floor is a slab on grade over about 2 feet of compacted fill. Except for two small areas at the ground floor, which are covered by one-story canopies, the plan configurations of each floor, including the roof, are the same. The floor system is reinforced concrete flat slab with thickness 10 inches at 2<sup>nd</sup> floor, 8.5 inches at 3<sup>rd</sup> to 7<sup>th</sup> floors and 8 inches at the roof (1 inch=2.54 cm). A penthouse, with mechanical equipment, covers approximately 10 percent of the roof area.

The interior partitions, in general, are gypsum wallboard on metal studs. Cement plaster, 1 inch thick, is used for exterior facing at each end of the building and at the stair and elevator bays on the long side of the building. Double 16 gauge metal studs support the cement plaster. Some additional cement plaster walls are located on the south side of the building at the first floor. The north side of the building, along column line D, has four bays of brick masonry walls located between the ground and the second floor at the east end of the structure. Nominal 1-inch expansion joints, separate the walls from the underside of the second floor spandrels. Although none of the wall elements described are designed as a part of the lateral force-resisting system, they do contribute in varying degrees to the stiffness of the structure.

Geological data indicate that the site lies on recent alluvium. A typical soil boring shows the underlying soil to be primarily fine sandy silts and silty fine sands. The foundation system consists of 38 inch deep pile caps, supported by groups of two to four poured-in-place 24-inch-diameter reinforced concrete friction piles. These are centered under the main building columns. All pile caps are connected by a grid of beams. Each pile is roughly 40 feet long and has design capacity of over 100 kips (444.8 KN) vertical load and up to 20 kips (89 KN) lateral load.

### 3.2 Strong Motion Accelerograms

The first known strong motion records in the building date back to the 1971 San Fernando earthquake (Fig. 2). Then, the building had only three self contained triaxial AR-240 accelerographs, one in the south-eastern corner at ground level, one in the center of the fourth floor, and one in the south-western corner; on the roof.

The central recording system (CR-1 accelerograph; Fig. 4), was installed in the building prior to the 1987 Whittier-Narrows earthquake. It is operated by California Department of Mines and Geology (CDMG). Between 1987 and 1994, the CR-1 system was triggered by many local and distant larger events [2]. Here, we analyze recorded accelerations only from the 1987 Whittier-Narrows ( $M_L=5.9$ ), 1992 Landers ( $M_S=7.5$ ), 1992 Big Bear ( $M_L=6.5$ ) and 1994 Northridge ( $M_L=6.4$ ) events, at epicentral distances 41, 186, 149 and 1.5 km. The direction of strong motion arrivals from the Whittier-Narrows, Landers and Big Bear earthquakes are E 27°S, East, and E 1.5°S. The largest accelerations were those recorded during the 1994 Northridge earthquake. Table 1 summarizes selected parameters of the above earthquakes and their recordings.

Table 1 Selected earthquake and accelerogram  
Parameters describing the data used in this paper

Earthquake	Date	$M_L$	R	$\phi$	$L_{REC}$	$L_{PROC}$	$a_{H,MX}$	$a_{V,MX}$
			[km]	[deg]	[s]	[s]	[g]	[g]
San Fernando	02/09/71	6.6	22	22-62	59.5	59.5	0.25	0.17
Whittier-Narrows	10/01/87	5.9	41	117	43	22.7 <sup>+</sup> 43	0.16	-
Landers	06/28/92	7.5 ( $M_S$ )	186	90	79	43.0 <sup>+</sup> 79	0.04	0.007
Big Bear	06/28/92	6.5	149	91.5	43	22.6 <sup>+</sup> 43	0.01	0.007
Northridge	01/17/94	6.4	1.5	270-318 240-350	60	60.0	0.44	0.27

<sup>+</sup> data digitized by M.D. Trifunac from xerox copy of one page of film record, presented in CDMG data reports

$M_S$ –	surface wave magnitude	$L_{REC}$ –	length of recorded accelerogram
$M_L$ –	local wave magnitude	$L_{PROC}$ –	length of processed accelerogram
R–	epicentral distance	$a_{H,MX}$ –	peak horizontal acceleration
$\phi$ –	azimuth of wave arrival	$a_{V,MX}$ –	peak vertical acceleration

### 3.3 Description of Damage

Between 1972 and 1993, the building was shaken many times, but suffered no visible damage. During the San Fernando earthquake, the peak horizontal acceleration at the foundation level was 0.25g. Between 1972 and 1993, the largest peak acceleration (0.16g) was recorded during the 1987 Whittier-Narrows earthquake (see Table 1). During the 1994 Northridge earthquake, the peak ground acceleration was 0.44g and the building suffered considerable damage.

#### 3.3.1 Damage Caused by the 1971 San Fernando Earthquake

Structural damage from the San Fernando earthquake was minor. Epoxy was used to repair spalled concrete of the second floor beam column joints on the north side and east end of the building. The nonstructural damage was extensive, and about 80 percent of all repair cost was used to fix drywall partitions, bathroom tiles and plumbing fixtures. The damage was most extensive on the second and third floors and minimal at the sixth and seventh floors [1].

### 3.3.2 Damage Caused by the 1994 Northridge Earthquake and its Early Aftershocks

During the Northridge Earthquake, the building experienced significant damage. Serious structural damage occurred in the exterior longitudinal, south (A) and north (D) frames. Those were designed to take most of the lateral loads in the EW direction.

In Frame A (Fig. 5 bottom, south side), wide shear cracks appeared in columns A3, A4, A5, A7 and A8, just below the contact with the spandrel beam of the 5<sup>th</sup> floor. The cracks width was 5–10 cm on the surface of the column at A5F5 and A7F5, and more than 10 cm at A8F5 (A5F5 means frame A, column 5, spandrel beam of 5<sup>th</sup> floor. At all these locations, deformation (buckling) of the longitudinal bars (due to large motions) was evident. Large deformation of the longitudinal bars at A8F5 also caused deformation of the transverse reinforcement. There was no visible damage along column A6 of the frame A, although both adjacent columns, A5 and A7, were seriously damaged. The 1<sup>st</sup> floor of this frame was covered from the exterior, possibly hiding some minor damage. Minor cracks (width <1 cm), occurred at A9F3 and A9F5.

In exterior frame D, the width of shear cracks on the surface of the columns was moderate (0.2–1 cm; Fig. 5 top). These cracks had clearly a visible “x” shape at locations D5F4, D7F4, D7F5, D8F3, D8F4, D8F5. Column D1 cracked (width ~1 cm) vertically along the 3<sup>rd</sup> floor. Those cracks extended also into the spandrel beams at 3<sup>rd</sup> and 4<sup>th</sup> floors in the form of vertical cracks (width < 1 cm).

At the 1<sup>st</sup> floor of frame D, at columns D2, D3 and D4, the cracks appeared to have been caused by a “short column” effect, due to the brick wall, built up to 1/3 of the height of the columns in the first four bays. These cracks were 0.5–1 cm wide (Fig. 5 bottom). A diagonal crack (about 0.5 cm wide) occurred at D9F2. Small diagonal cracks (width less than 0.5 cm) were noticed at locations D6F2 and D7F2. In the brick walls, in the four eastern bays of the first floor, cracks occurred between the bricks (through mortar), at the upper corners of the walls (Fig. 5 top).

There was no visible damage to the interior longitudinal frames (B and C), although some cracks could have been hidden by large furniture (especially on the first floor), wallpaper and carpets. No damage was observed in the reinforced concrete slabs. Small cracks (width < 0.2 cm) were noticed in the slab around the central columns on 5<sup>th</sup> and 6<sup>th</sup> floors. There were no signs of large deformations in the foundation, neither at the 1<sup>st</sup> floor slab nor in the pavement around the building.

The nonstructural damage was extensive. Every guest room suffered some type of nonstructural damage. Furniture was overturned at the upper floors (above 3<sup>rd</sup>). Due to large relative motions and deformation of the interior walls, the wallpaper was distorted or torn off. The relative displacements also caused extensive damage to the brittle ceramic tile covers in the bathrooms. There were numerous cracks in the bathtubs, and many ceramic tiles fell off.

### 3.4 Wave Propagation In and Around the Building

In the following, we analyze the accelerograms recorded in the building, using simple approximate representation based on wave propagation. Figure 2 shows the setting of the building, in central San Fernando Valley, and the horizontal projections of the 1971 San Fernando and 1994 Northridge earthquake faults. During the San Fernando earthquake, the faulting started at depth, ~ 9 km below surface, and propagated up and towards south with average dislocation velocity of ~2 km/s, along the fault plane dipping 40° and striking N72W [16]. The consequence of this propagation is that the waves arrived at the building site first at angle  $j = 22^\circ$ , and then  $j$  increased towards 62°, during the following 9 s (Fig. 2). The strongest motion arrived from the deep part of the dislocation surface, during the first 4 seconds, and then from the shallow part of the fault during the last two seconds of faulting.

The fault motion for the Northridge earthquake [21] is shown by snapshots of fault dislocations with time increments of one second. The open empty ovals, the darker vertically hatched zones and the dark horizontally hatched zones show respectively areas with dislocation amplitudes >0.5, 1.0 and 1.5 m. It is seen that the largest dislocations propagated towards NW, during the first 5 seconds, and then, only during the last second, towards West, with dislocation velocity 2.8–3 km/s. Assuming that most of the strong motion energy arrived from the area

with largest dislocation amplitudes, implies wave arrivals with azimuths  $j = 270\text{--}318^\circ$ . However, because the entire fault surface radiated energy, the range of azimuths for wave arrivals was actually broader,  $j = 240\text{--}350^\circ$ .

During the Whittier-Narrows, Landers and Big Bear earthquakes, the building was at epicentral distances 41, 186 and 149 km. Because of the small fault dimensions relative to the corresponding epicentral distances, in laterally homogeneous layered earth (Fig. 6a,b), all the wave energy would have been arriving along essentially same respective paths. However, the complex geologic structure (the Santa Monica and Verdugo Mountains, and the Elysian and Repetto Hills are between San Gabriel and Los Angeles Valleys) contributed to lateral scattering resulting in more complicated multiple direction arrivals of wave energy towards the building.

Figure 7 shows a schematic vertical cross-section through the focus of the Northridge earthquake and the building site (see Fig. 2). It is seen that for the waves arriving first towards channel 1 and then towards channel 13 (40 m apart, at the western and eastern ends of the building), the SH- and Love-wave components of the early motions could be delayed for these two channels by  $\Delta t \leq 0.05$  sec. Direct body waves would be delayed less (due to large radial phase velocity  $C_R$ ), while the waves traveling through shallow low velocity layers would be delayed at most by  $\Delta t \approx 0.05$  sec. About 5 to 6 s later, the energy originates near the NW end of the fault, at depth  $\approx 10$  km, and at distance  $\approx 15$  km NW from the building site. For azimuths  $j = 318\text{--}350^\circ$ , the “separation distance” for channels 1 and 13 decreases to  $\approx 27$  and 7 m respectively, and this reduces the relative delay of wave arrivals at channels 13 and 1 to  $\Delta t \approx 0.008$  s or less. Following the direct arrivals from the fault plane, the surface and coda waves of strong motion may arrive from all directions, scattered and reflected from the edges of sediments in San Fernando Valley.

### 3.5 Required Accuracy in Data Processing

For the above delays to be seen in recorded data, it is necessary to have accurate relative timing of the data recorded by different channels of the CR-1 recording system. This requires (1) accurate digitization of the beginning of all traces, and (2) accurate corrections for variations in film speed. Our routine accelerogram processing software produced corrected data (for baseline and instrument response) equally spaced at 50 points/s until the early 1990's, and currently at 100 points/s. It is seen that the expected “delays” between motions at channels 1 and 13 due to wave propagation (see Fig. 4) are  $\approx 0.01\text{--}0.03$  s  $\approx 1$  to several intervals of equally spaced points at  $\Delta t = 0.01$  s.

To evaluate the relative accuracy of time coordinates of the Northridge earthquake record digitized by CDMG, we redigitized independently the same record, from a reproduction of the film record in reference [8]. By visual comparison of the first several seconds of digitized data, and by cross-correlation analysis, we found that CDMG digitization “omits” (starts late) up to  $\sim 0.03$  s at the beginning of some traces. In Fig. 8, we document these “omitted” intervals for all 13 channels for this record. It is seen that the origin times of both digitizations agree for channels 1 and 2. The CDMG data begins progressively late with increasing channel number, and the delay is  $\approx 0.02$  s for channels 8 through 13. For channel 12, the delay is the largest ( $\approx 0.03$  s).

Figure 9 shows similar comparison of initial delays for three other earthquakes (Whittier-Narrows, Big Bear and Landers). It is seen that the differences are of systematic and repetitive nature. Though there are several simple and plausible explanations for these differences, we cannot state their cause with certainty. As an illustration only, we suggest that one possible explanation can be related to different optical densities of different traces on the film, when digitized with same threshold level of gray [4, 18].

### 3.6 Rough Estimation of Apparent Travel Times

An approach to investigating the wave propagation inside the building may be formulated starting with the assumption that the incident energy consists of pulses, which then propagate from one recording point to another. To find the time delay representing the average difference at stations  $i$  and  $j$  of all arrival times collectively, we can evaluate cross-correlation functions of the recorded motions,  $R_{ij}(t)$ , where  $t$  represents the average delay or “travel time”. To emphasize the local pulses and to avoid randomization caused by numerous pulses during the entire

excitation history, we multiply recordings at stations  $i$  and  $j$  by windows,  $W(t)$ , as shown in Fig. 10. These windows have unit amplitude in a 2 s interval, 0.5 s ramps on each side, and zero amplitudes otherwise. Then we compute

$$R_{i,j}(t_0, \tau) = \int_{t_0}^{t_0+\tau+3} f_i(t)W(t-t_0)f_j(t+\tau)W(t-t_0-\tau)dt \quad (4)$$

and find the delay  $t_0$  for which the amplitude of  $R_{ij}(t_0, \tau)$  is maximum. The physical interpretation of the result and the estimates of  $t_0$  depend on the assumed properties of the window function  $W(t)$ . Analysis of these properties is beyond the scope of this paper. Here, for simplicity and to illustrate the general trends, we adopt only one window function  $W(t)$ , as shown in Fig. 10. Figures 11 through 12 show plots of  $t_0$  versus  $t_0$  only for the NS accelerations in the building recorded during the Whittier-Narrows, Landers, Big Bear and Northridge earthquakes.

Forward evaluation of the average shear-wave velocity in the building requires representation of the structure by at least two types of anisotropic layers with different properties [14], one for the floor slabs and one for the columns. It also requires estimation of the relative fixity of the columns. Details of this modeling are beyond the scope of this paper. Here, we only state that such analysis shows that the velocity of vertically propagating shear-waves in this building is  $\approx 100$  m/s, and that the velocity of SH- waves along the floor slabs is  $\approx 2000$  m/s. These estimates are consistent with the experimental results presented here, and with other independent analyses of wave motion in this building, which will be presented in future papers.

Assuming plane vertically propagating waves, with average shear-wave velocity in the vertical direction  $b=100$  m/s would imply  $t_0 = h_{ij}/100$ , where  $h_{ij}$  is the vertical separation of stations  $i$  and  $j$  (in meters). In Figs 11 and 12 (left and right columns), these propagation times are shown by thin dashed lines. The computed  $t_0$  delays are shown by heavy interrupted lines. Occasionally, reflections off the top or off the sides of the building may cause peaks of  $R_{ij}(t_0, \tau)$  to occur at much longer or shorter  $t_0$  than what we assume corresponds to the direct waves. To simplify this presentation, we chose not to show those values.

The central columns in Figs 11 and 12, show time delays,  $t_0$ , of pulses propagating along the longitudinal axis of the building, in the EW direction. Complete interpretation and modeling of what those delays represent is a complex problem whose analysis is beyond the scope of this paper. Assuming that the building has to follow the ground motion [14] and ignoring soil structure interaction, would lead to  $t_0$  for  $R_{1,13}$  to depend on the average travel time of shear-waves and of horizontal components of P, SV and Rayleigh waves in the soil between locations of channels 1 and 13. For EW propagation, these two locations are 40 m apart, but for other directions of wave approach, this distance can be anything between 0 and 40 m. For the Whittier-Narrows, Landers and Big Bear earthquakes, most of the energy traveled from East to West (see Fig. 2) and so  $t_0$  must be negative (see eqn 4). Between 5.5 and 7.0 s after trigger, the records of Whittier-Narrows earthquake show shear-wave arrivals which should be associated with “high” values of phase velocities, and  $t_0$  should be “small” and negative (Fig. 13). Twelve seconds after trigger, the recorded motions show arrival of surface waves and  $t_0$  for  $R_{1,13}$  is in the range from  $-0.04$  to  $-0.08$  s, suggesting phase velocity between 0.5 and 0.95 km/s. These values are “reasonable” for intermediate and high frequency ( $f > 1$  Hz), first and second modes of surface Love waves in San Fernando Valley (e.g. Fig. 6b).

For the Landers earthquake, the largest earthquake of the four considered here,  $t_0$  for  $R_{1,13}$  is negative and “small”, and is constant throughout the entire duration of wave arrival (Fig. 13). This suggests predominantly surface waves with strong participation of long periods and higher modes, contributing with phase velocities  $c = 2.15$  to 3.5 km/s. During the Big Bear earthquake, the accelerations at the building site were small, and the instruments triggered late, apparently after the arrival of shear waves. The motion appears to be dominated by high frequency surface waves with phase velocities  $c = 0.5$  to 0.95 km/s, during the first 12 s of recorded motion (Fig. 13). Between 12 and 20 s, the waves appear to be associated with larger EW and NS motions, suggesting arrivals from all directions and SH components arriving from North or South. This would reduce the apparent separation distance between the recording sites for channels 1 and 13, resulting in small values of  $t_0$ .

During the first 12 s of the Northridge earthquake, the waves arrived first from west and then later from north-west (see Fig. 2 and 7) resulting in positive  $t_0$  in  $R_{1,13}$ . With time, as the predominant direction of wave approach changed from West to NW, the effective separation of stations 1 and 13 decreased, thus leading to gradual decrease of  $t_0$ . Beyond 12 to 15 s, the motion most probably arrived from “all” directions representing scattered and reflected

waves from irregular geologic boundaries of San Fernando Valley, and this resulted in small values of  $t_0$ . These trends and variations of  $t_0$  versus  $t_0$  (Fig. 13) can be seen also at the 2<sup>nd</sup> ( $R_{7,8}$ ), 3<sup>rd</sup> ( $R_{5,6}$ ) and 8<sup>th</sup> ( $R_{2,3}$ ) floors of the building, but other effects caused by wave reflections off the East and West ends of the building are superimposed (see Fig. 11 and 12). We show these results for completeness of this presentation, but leave the detailed analyses and interpretation for future work.

The above results on  $t_0$  in  $R_{ij}(t_0, t_0)$  are based on USC digitalization and processing of CR-1 and SMA-1 records (using xerox copies of the records published in CDMG reports). After digitization and processing, to achieve internally consistent and physically plausible results, in Fig. 11 and 12, it was necessary to shift (advance) the origin time of different components (channels) as shown in Fig. 14. These shifts are small relative to the significant prolongations of  $t_0$  for  $R_{5,2}$  and  $R_{6,4}$ , seen only for the Northridge data (Fig. 12 bottom). The required shifts for the Big Bear earthquake however are surprisingly large.

The Big Bear acceleration records began with a late trigger (during arrival of surface waves and after the S-wave arrival). The amplitudes are small and the traces achieved full optical density after more than about 0.1 s. It is possible that the unexpected pattern of “required” shifts is caused by artificial reduction of trace width (and thus loss of the trace beginning) by the high contrast characteristics of xerox copying. This effect may apply to both USC and CDMG digitalizations, to a similar degree, such that a relative starting time between these two digitalizations (see Fig. 9) still applies. Further analysis and interpretation of this interesting and important data processing problem [18] is however beyond the scope of this work.

Large reduction of “propagation velocities” is seen only in the values of  $t_0$  for  $R_{5,2}$  and  $R_{6,4}$ , during the Northridge earthquake. As Fig. 12 (bottom) shows, the computed  $t_0$  is roughly two times longer than expected. With reference to Fig. 5, it is possible to speculate that this is caused by damage of the columns just below the spandrel beams on the 5<sup>th</sup> floor.

#### 4. DISCUSSION AND CONCLUSIONS

We explored the possibility of measuring propagation velocity of waves in a simple symmetric structure, and interpreting the observed delays in wave arrivals as indicators of damage [7]. We computed the propagation “time” from a pair of stations by using windowed cross-correlation function. This rough method ignores wave dispersion and the presence of “other” reflecting boundaries, and therefore is contaminated and can give wrong answers in the presence of many reflections. Nevertheless, the results we obtained show promise and appear to give significantly long travel times in the areas where damage did occur.

The first requirement for the success of this method is that the time coordinates of processed strong motion data must be (1) as accurate as possible and (2) their accuracy must be analyzed, interpreted and quantified. Since we are able to identify the first digitization point for each acceleration trace with accuracy of about one pixel (e.g. for scanners with 600 dpi the width of one pixel is 1/236 cm, that is 0.004 sec), it is necessary only to calibrate the accuracy of electrical signals creating two pulses per second (2 PPS) time trace, which is usually written on the edge of the film. For digital instruments, in principle, neither the starting nor relative timing of samples from different channels should pose problems, but the actual speed of multiplexing, and the frequency of sampling must be accurately measured and should be documented.

In this study we use the concept of equivalent continuous medium to represent a three-dimensional structure, but for accurate identification of damaged zones the modeling of structures may have to be more detailed. The difficult and challenging task will be to develop digital filters which can account for various scattered waves and for reflections in a three-dimensional matrix of structural members, which will then be used to measure the “wave” velocity between the two points.

Finally, we mention the obvious limitation of the above method. It has to do with its ability to resolve “small” and concentrated damage zones. The method can offer only an order of magnitude ( $\sim N$ ) improvement over measurements of changes in natural frequencies. It is, of course, possible in principle to saturate buildings with

transducers, densely distributed, on all structural members, but this is obviously not a practical alternative. The best we can expect, at present, is to have one instrument per principal direction per floor. This will correspond to approximately three times better resolution than in the example presented in this paper.

## 5. REFERENCES

1. Blume, J.A. and Assoc. (1973). Holiday Inn, Chapter 29 in "San Fernando, California Earthquake of February 9, 1971," Volume I, Part A, U.S. Dept. of Commerce, National Oceanic and Atmospheric Administration, Washington, D.C.
2. Graizer, V.M. (1997). Personal Communication.
3. Ivanovic, S. and M.D. Trifunac (1995). Ambient vibration survey of full scale structures using personal computers (with examples in Kaprielian Hall), Dept. of Civil Engrg, Rep. No. 95-05, Univ. of Southern California, Los Angeles, California.
4. Lee, V.W. and M.D. Trifunac (1990). Automatic digitization and processing of accelerograms using PC, Dept. of Civil Engrg, Rep. No. 90-03, Univ. of Southern California, Los Angeles, California.
5. Luco, J.E., H.L. Wong and M.D. Trifunac (1986). Soil-structure interaction effects on forced vibration tests, Dept. of Civil Engrg, Report No. 86-05, Univ. of Southern California, Los Angeles, California.
6. Moslem, K. and M.D. Trifunac (1986). Effects of soil structure interaction on the response of buildings during strong earthquake ground motions, Dept. of Civil Engrg, Report No. 86-04, Univ. of Southern California, Los Angeles, California.
7. Safak, E. (1998). Detection of seismic damage in multi-story buildings by using wave propagation analysis, Proc. Sixth U.S. National Conf. on Earthquake Eng., Seattle, Washington.
8. Shakal, A., M. Huang, R. Darragh, T. Cao, R. Sherburne, P. Malhotra, C. Cramer, R. Syndov, V. Graizer, G. Maldonado, C. Peterson and J. Wimpole (1994). CSMIP strong motion records from the Northridge, California, Earthquake of 17 January 1994, Report No. OSMS 94-07, Calif. Dept. of Conservation, Div. Of Mines and Geology, Sacramento, California.
9. Todorovska, M.I. and M.D. Trifunac (1989). Anti-plane earthquake waves in long structures, J. Engrg Mechanics, ASCE, 115(12), 2687-2708.
10. Todorovska, M.I. and M.D. Trifunac (1990). A note on excitation of long structures by ground waves, J. Engrg Mechanics, ASCE, 116(4), 952-964.
11. Todorovska, M.I. and M.D. Trifunac (1990). Propagation of earthquake waves in buildings with soft first floor, J. Engrg Mechanics, ASCE, 116(4), 892-900.
12. Todorovska, M.I. and M.D. Trifunac (1990). Analytical model for the in-plane building-foundation-soil interaction: incident P-, SV-, and Rayleigh waves, Dept. of Civil Engrg, Report No. 90-01, Univ. of Southern California, Los Angeles, California.
13. Todorovska, M.I. and M.D. Trifunac (1991). Radiation damping during two-dimensional in-plane building-soil interaction, Dept. of Civil Engrg, Report No. 91-01, Univ. of Southern California, Los Angeles, California.
14. Todorovska, M.I., V.W. Lee and M.D. Trifunac (1988). Investigation of earthquake response of long buildings, Dept. of Civil Engrg, Report No. 88-02, Univ. of Southern Calif., of Los Angeles, California.
15. Trifunac, M.D. (1972). Comparison between ambient and forced vibration experiments, Earthquake Engrg and Struct. Dynam., 1, 133-150.
16. Trifunac, M.D. (1974). A three-dimensional dislocation model for the San Fernando, California, Earthquake of February 9, 1971, Bull. Seism. Soc. Amer., 64, 149-172.
17. Trifunac, M.D., S.S. Ivanovic and M.I. Todorovska (1999). Experimental evidence for flexibility of foundation supported by concrete friction piles, Soil Dynam. and Earthquake Engrg, 18(3), 169-187.
18. Trifunac, M.D., M.I. Todorovska and V.W. Lee (1999). Common problems in automatic digitization of strong motion accelerograms (submitted for publication).
19. Udawadia, F.E. (1977). Uniqueness problems in structural identifications from strong motion records, Proc. Sixth World Conf. On Earthquake Engrg, Sarita Prakasan, Meerut, India, Vol. II, 1010-1015.
20. Udawadia, F.E. and M.D. Trifunac (1974). Time and amplitude dependent response of structures, Earthquake Engrg and Struct. Dynam., 2, 359-378.
21. Wald, D.J. and T.H. Heaton (1996). The slip history of the 1994 Northridge, California, earthquake determined from strong-motion, teleseismic, GPS and leveling data, Bull Seism. Soc. Amer., 86(1B), S49-S70.

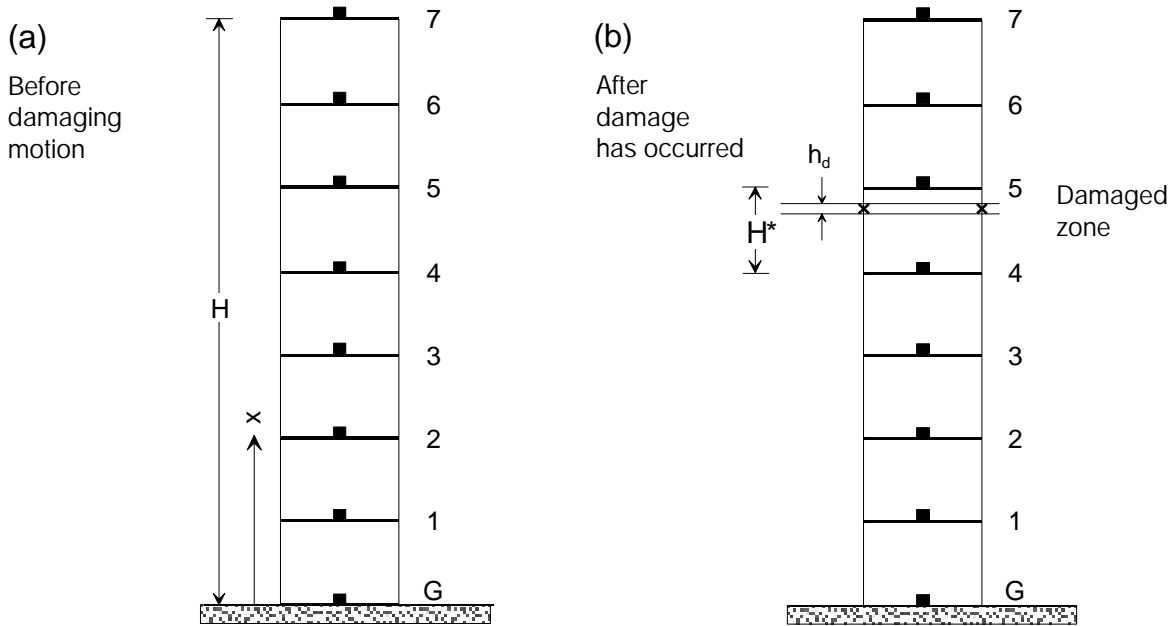


Figure 1. A multi degree-of-freedom system (a) before and (b) after localized damage has occurred (e.g. in the columns below the 5<sup>th</sup> floor). The solid squares indicate locations of the strong motion instruments.

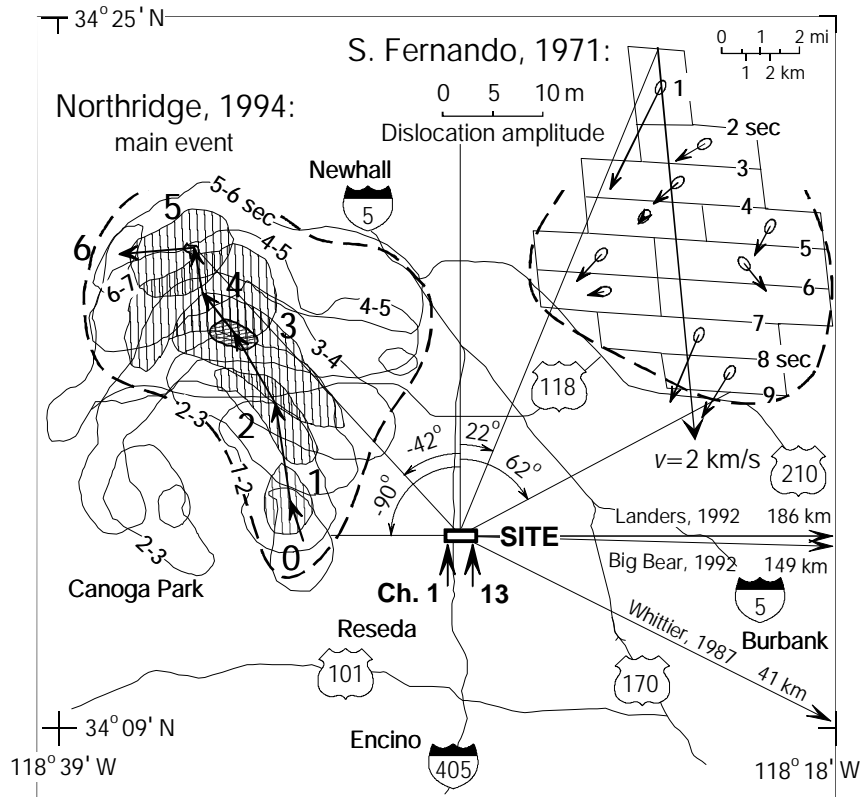


Figure 2. San Fernando Valley area showing the site of the 7-storey hotel relative to the fault planes of 1971 San Fernando and 1994 Northridge earthquakes. Directions toward the 1987 Whittier-Narrows, 1992 Landers and 1992 Big Bear earthquakes are shown by arrows.

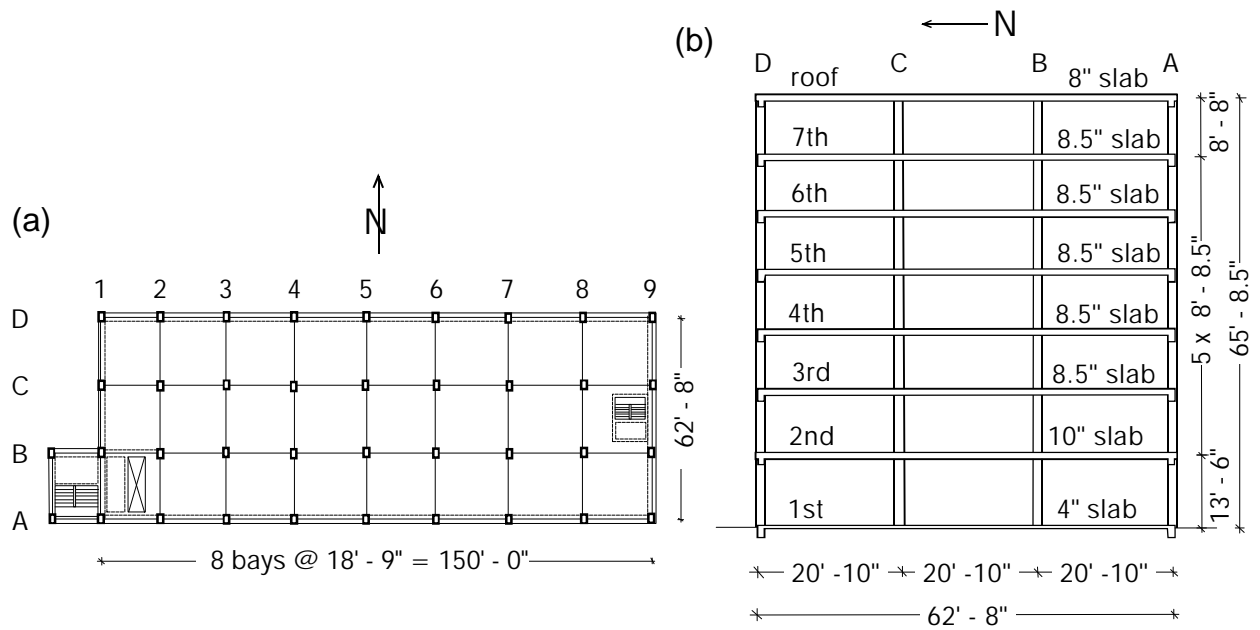


Figure 3 (a) A typical floor plan, and (b) a typical transverse section for the 7-storey hotel.

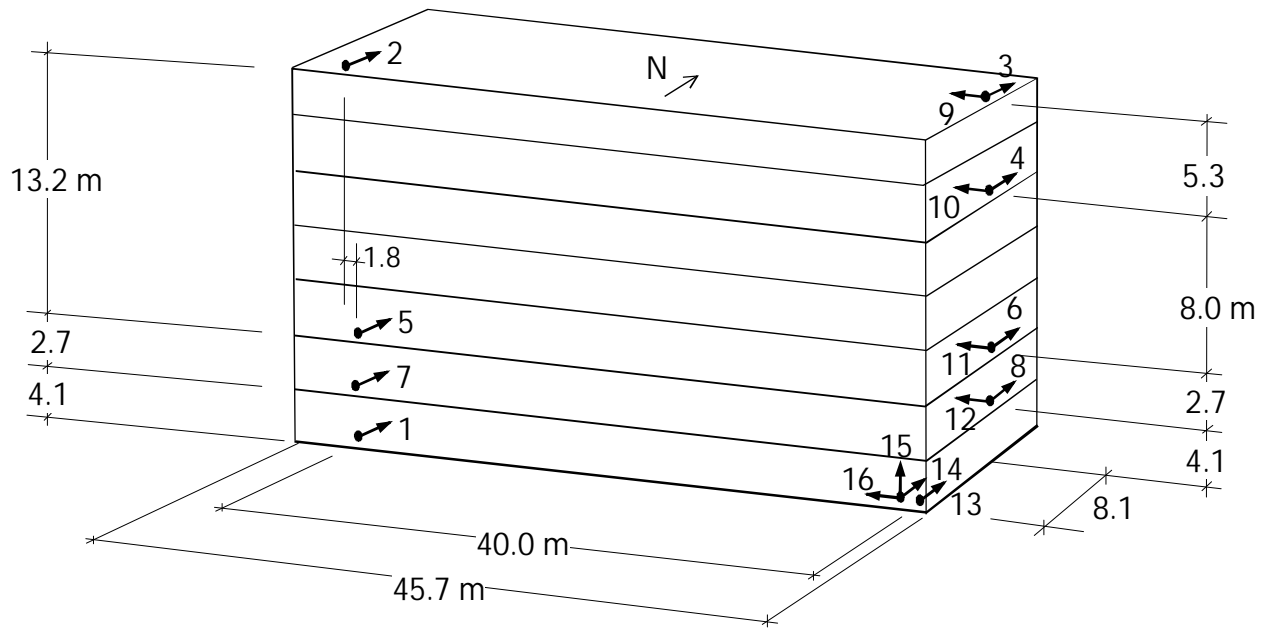


Figure 4. Sensor locations and orientations for the CR-1 recording system (channels 1–13) and for the SMA-1 accelerograph (channels 14–16).

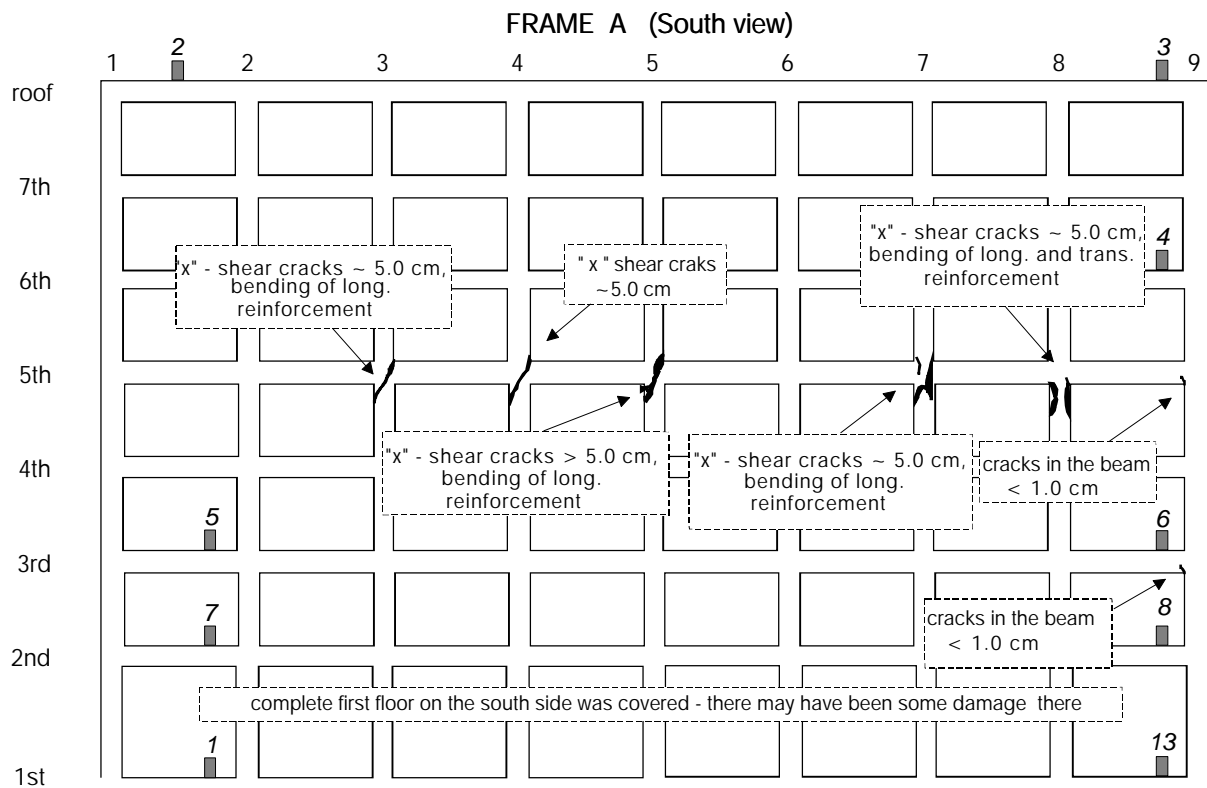
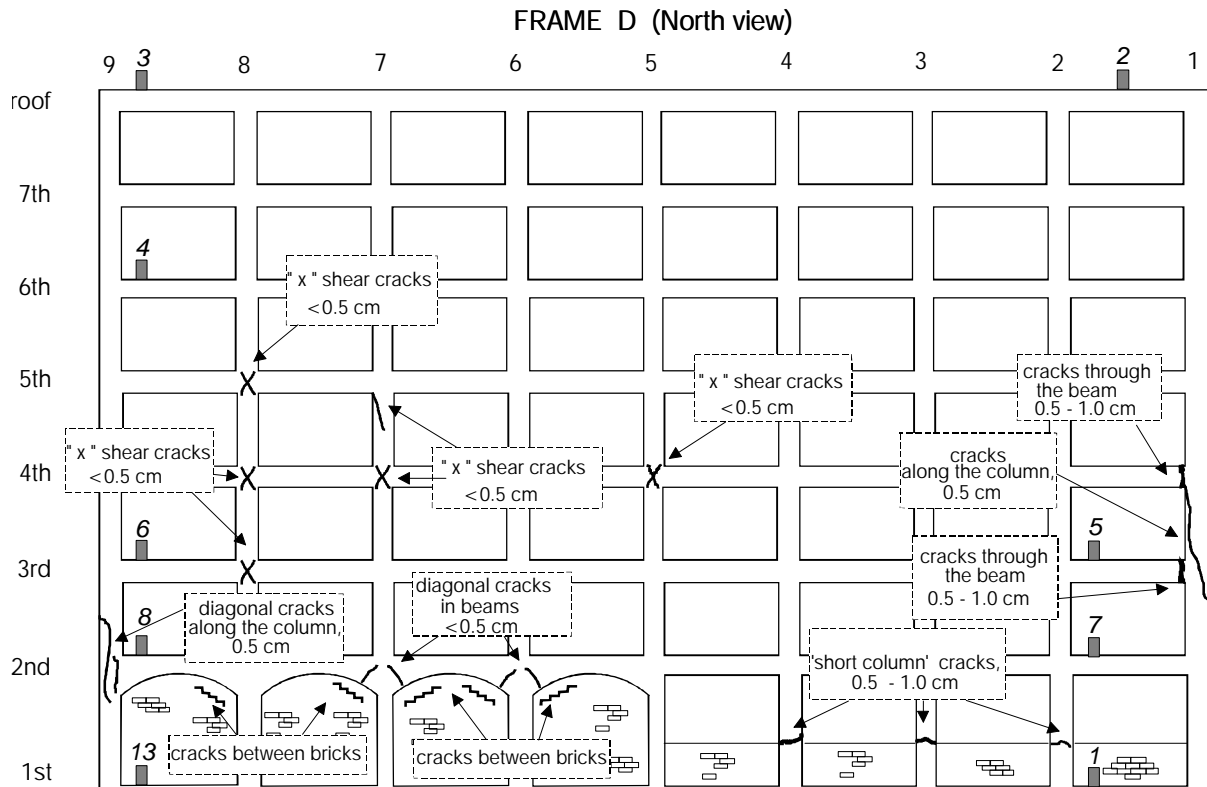


Figure 5. Schematic representation of damage: (top) frame D (North view), and (bottom) frame A (South view). The sensor locations for channels 1–8 and 13 (oriented towards North), are also shown (see also Figure 4).

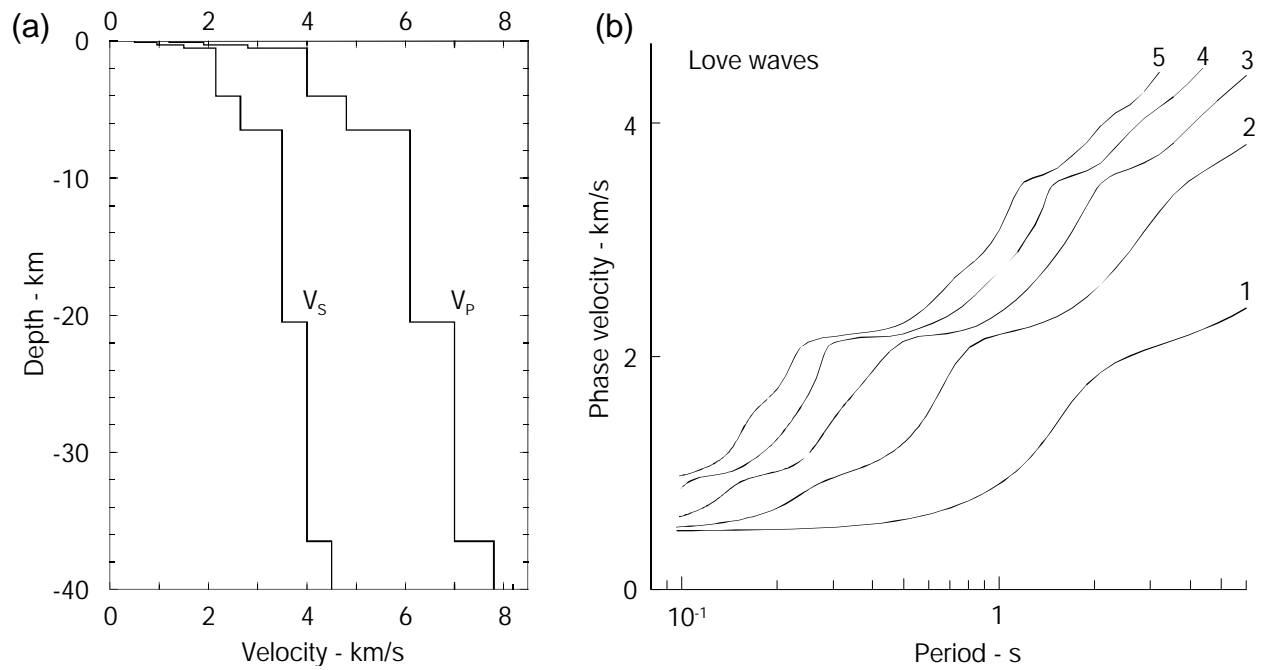


Figure 5. Schematic representation of damage: (top) frame D (North view), and (bottom) frame A (South view). The sensor locations for channels 1–8 and 13 (oriented towards North), are also shown (see also Figure 4).

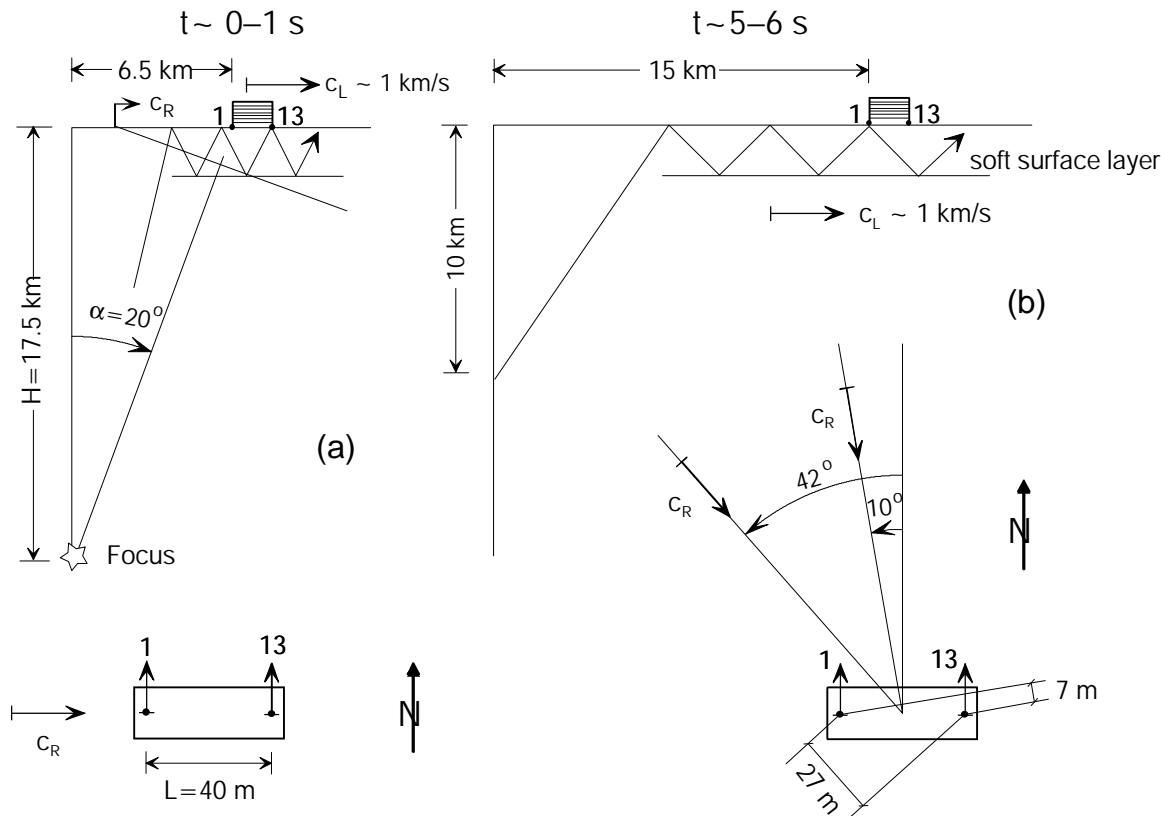


Figure 7 An illustration of predominant wave arrivals from the rupture of the 1994 Northridge earthquake (Figure 2). Parts (a) and (b) show vertical cross-sections through the building site, at the beginning ( $\sim 0-1$  s) and towards the end ( $\sim 5-6$  s) of the main dislocation sequence. Note the propagation of energy predominantly towards east in part (a), and predominantly towards south-east in part (b).

# Van Nuys, 7-storey Hotel

Northridge Earthquake, 17 Jan. 1997, 12:30 GMT,  $M_L=6.4$ ,  $H=18$  km

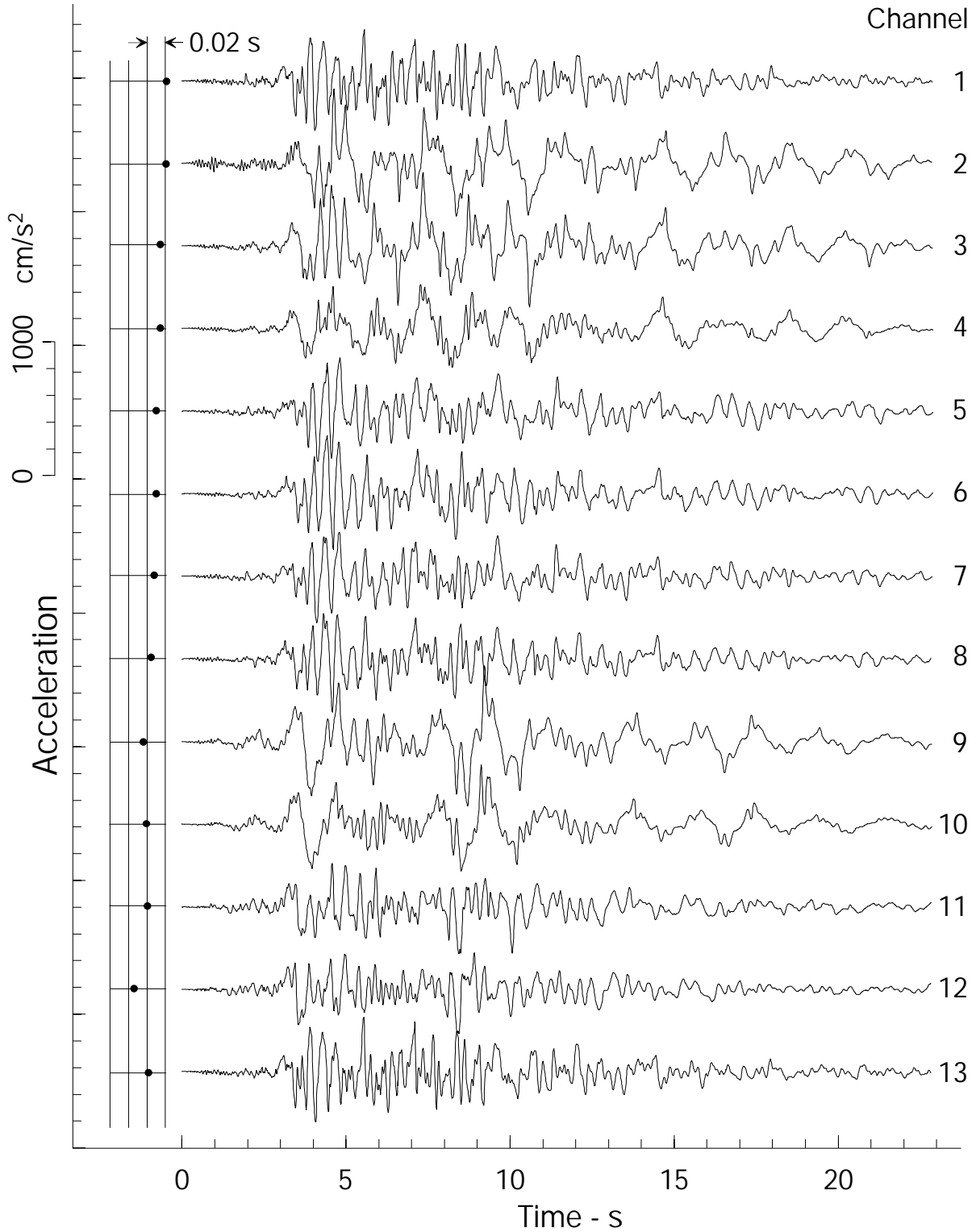


Figure 8. Recorded strong motion accelerations and time delays for the 13 CR-1 channels digitized by CDMG, relative to the same data digitized by USC. The delay is the largest for Channel 12 ( $\sim 0.03$  s).

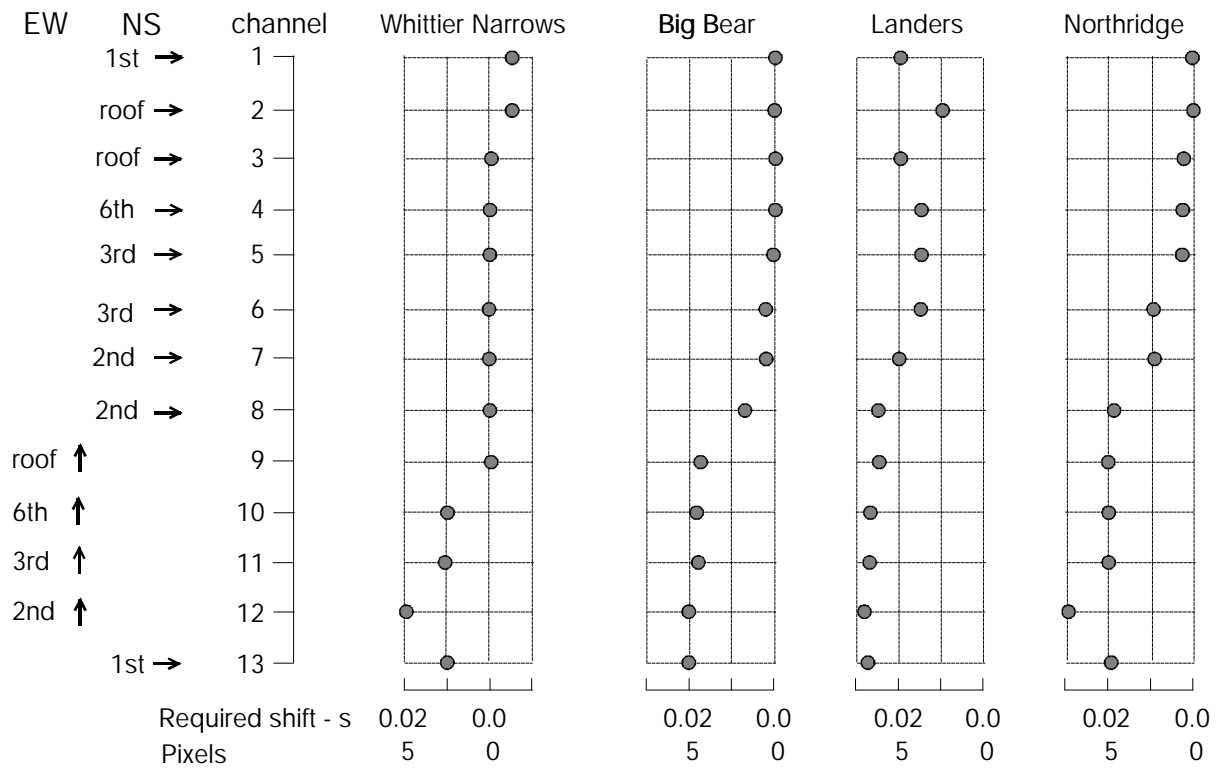


Figure 9 Time delays (in seconds and pixels) for the CDMG-digitized data of the 13 CR-1 channels, relative to the USC-digitized data, for the records of the 1987 Whittier-Narrows, 1992 Big Bear, 1992 Landers and 1994 Northridge earthquakes.

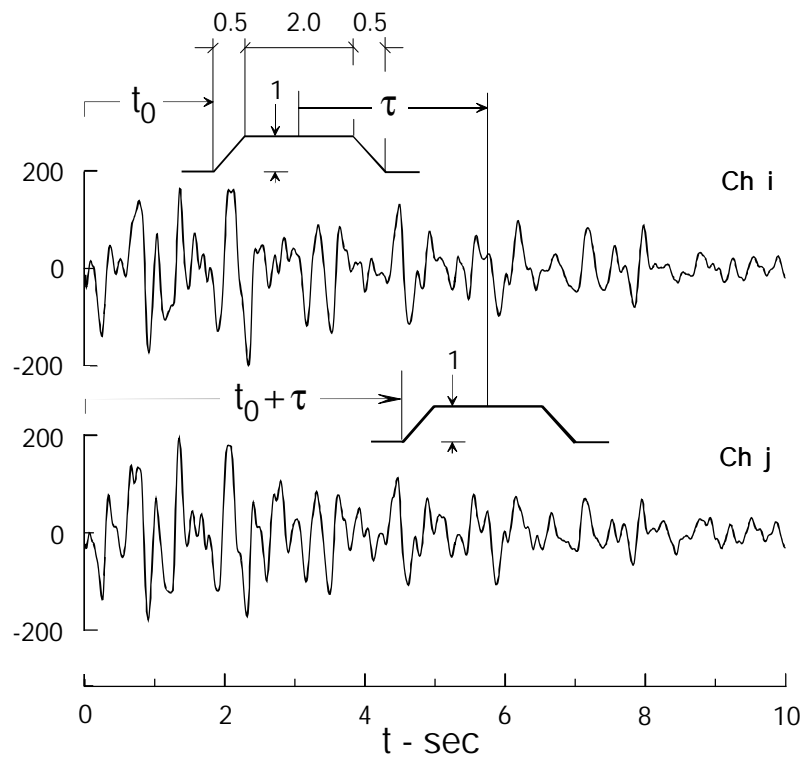


Figure 10 An illustration of the time windows applied to a pair of signals (channels i and j), and the delay,  $\tau$ , as used in computing the cross-correlation function of the two acceleration signals,  $R_{ij}(t_0, \tau)$  (see Figures 11 and 12).

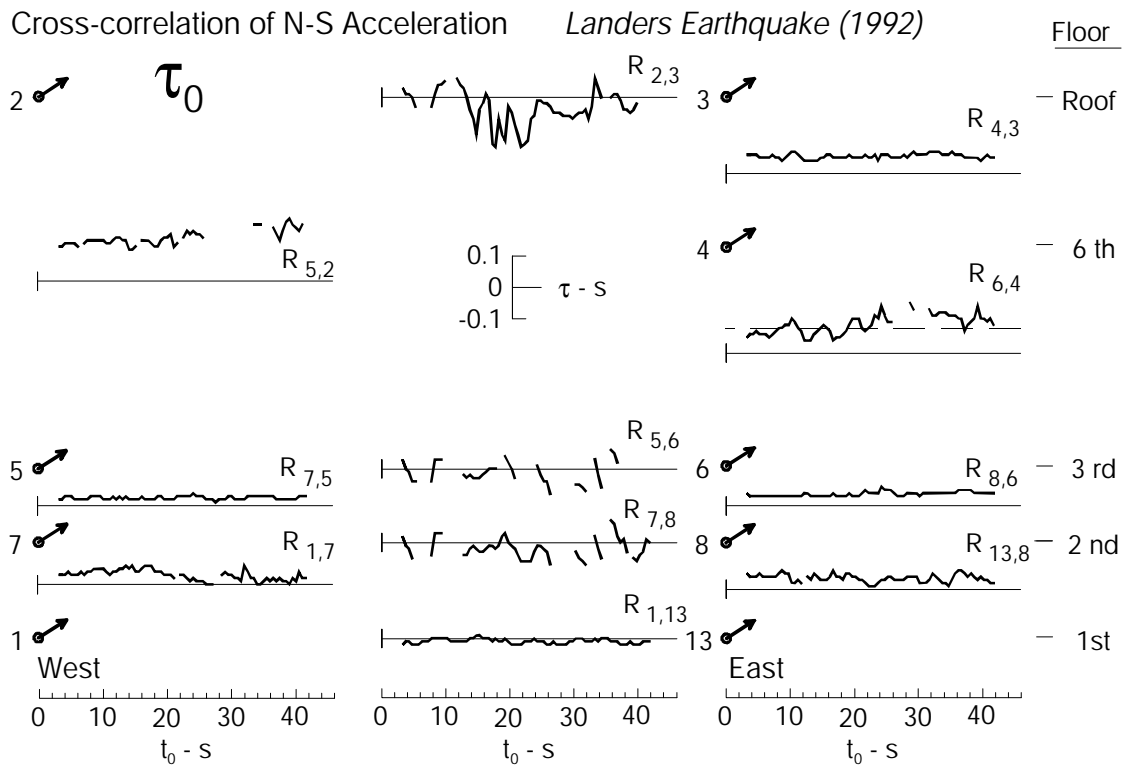
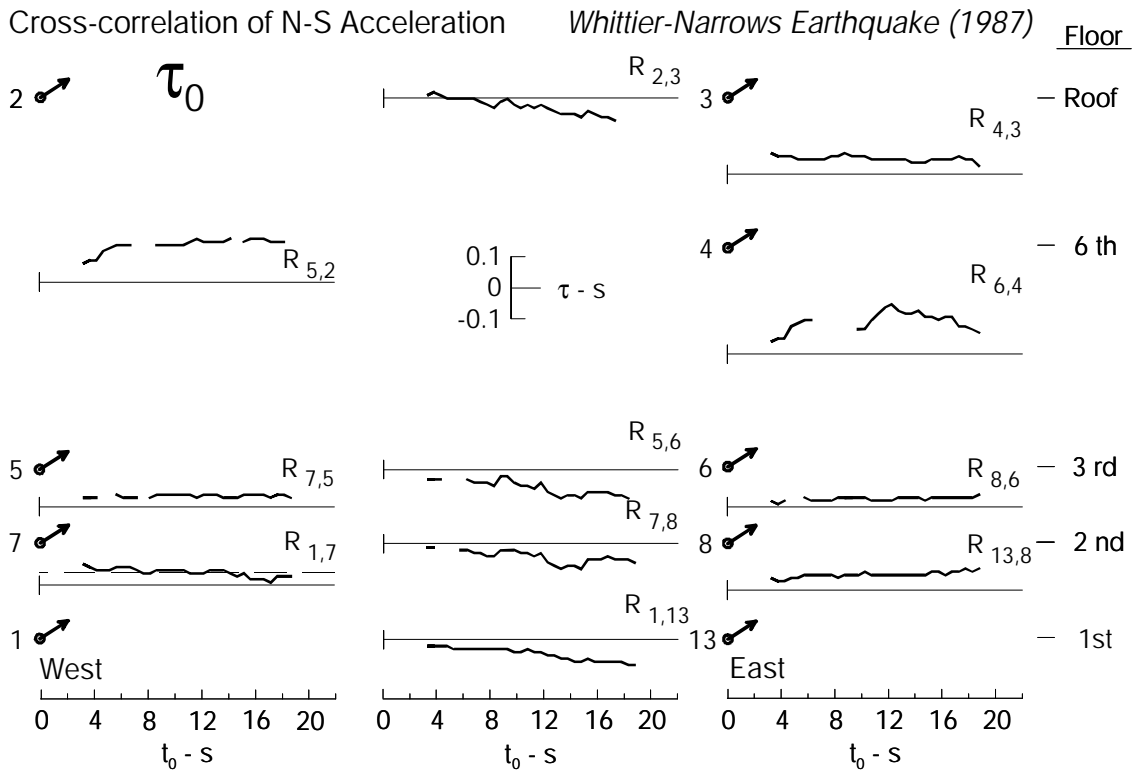


Figure 11 Delay,  $\tau = \tau_0$ , for maximum cross-correlation,  $R_{ij}(t_0, \tau)$ , versus time  $t_0$  (see Figure 10), for recorded N-S accelerations during the 1987 Whittier-Narrows (top) and 1992 Landers (bottom) earthquakes.

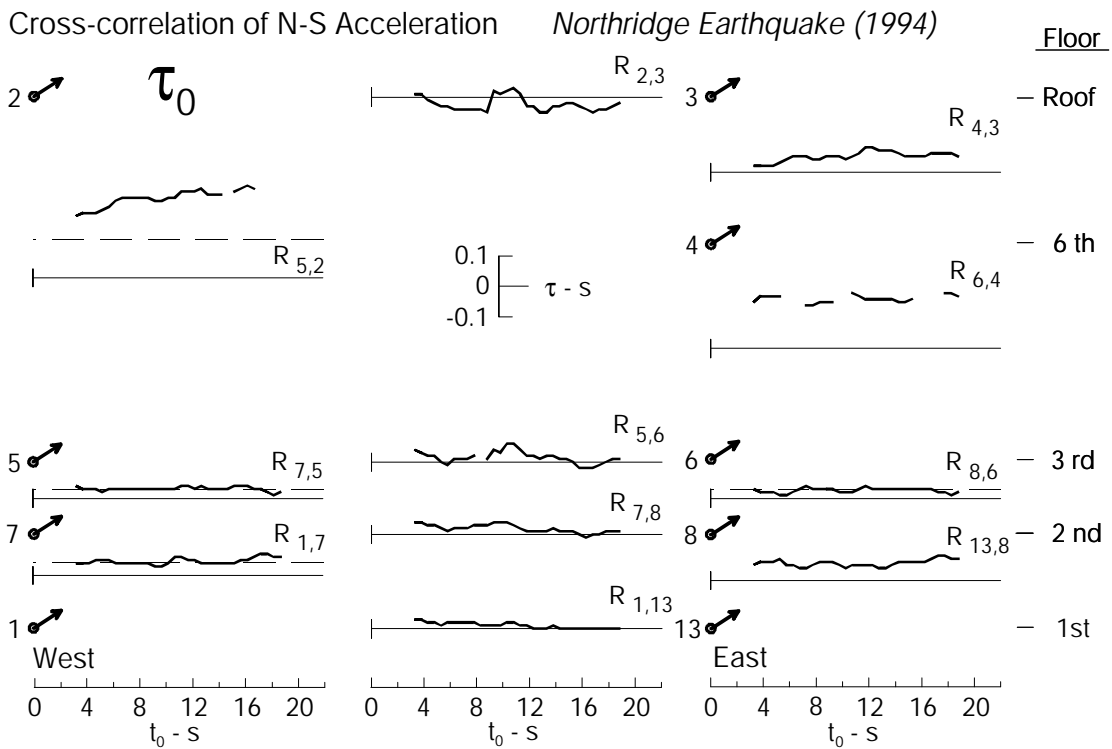
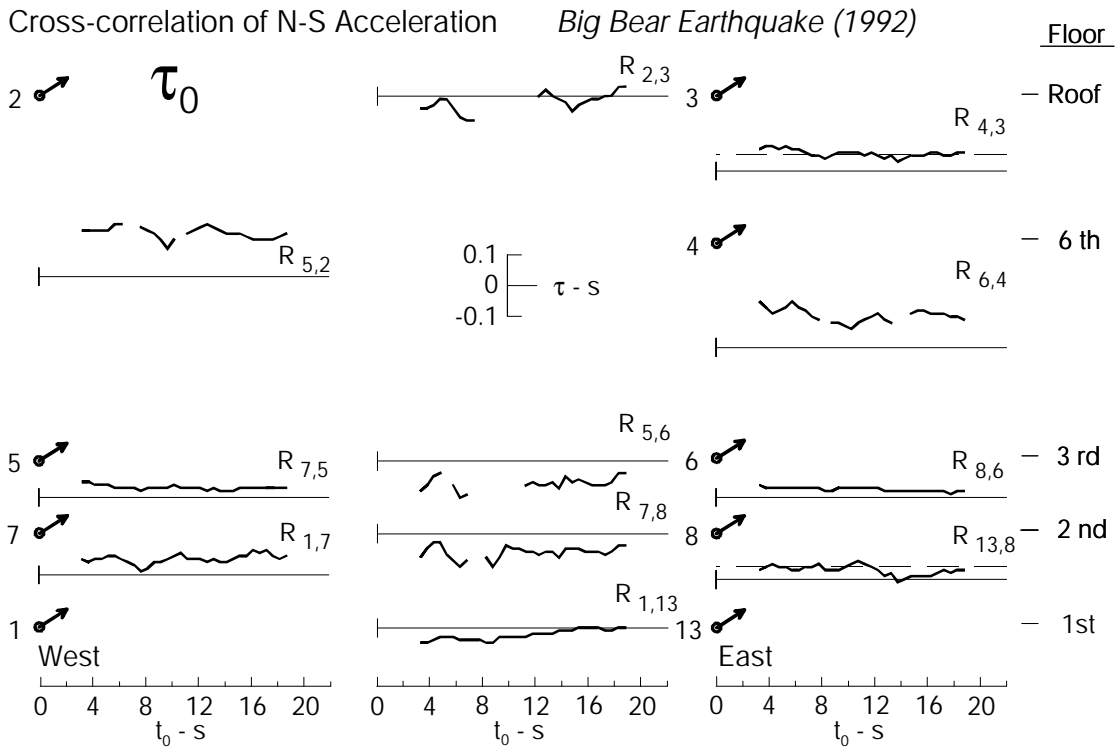


Figure 12 Delay,  $\tau = \tau_0$ , for maximum cross-correlation,  $R_{ij}(t_0, \tau)$ , versus time  $t_0$  (see Figure 10), for recorded N-S accelerations during the 1992 Big Bear (top) and 1994 Northridge (bottom) earthquakes.

### Cross-correlation of N-S Acceleration $R_{1,13}$

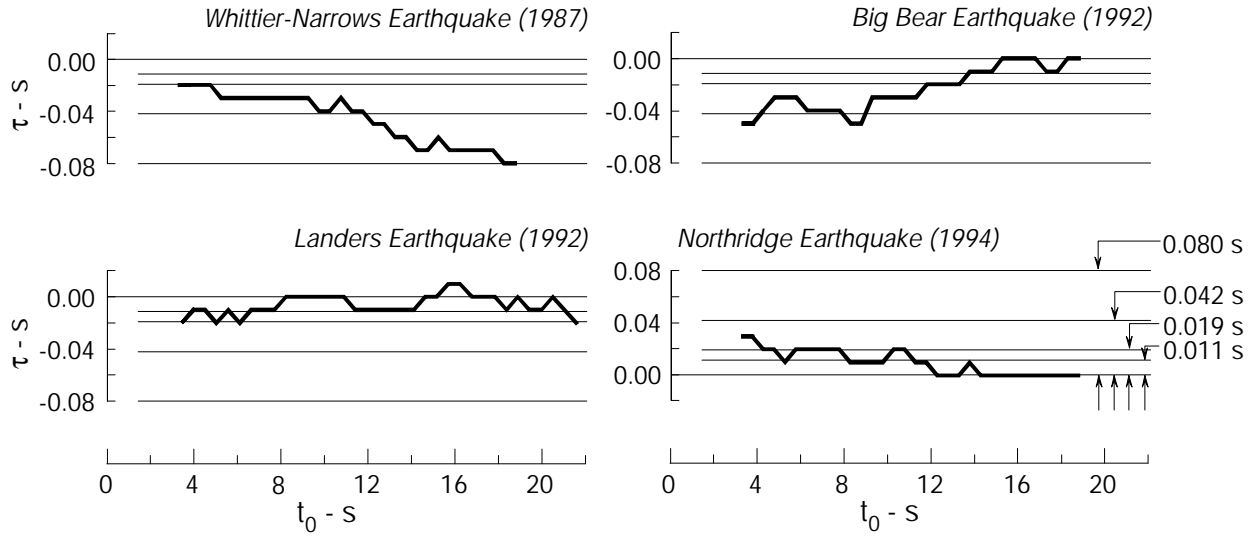


Figure 13 Delay,  $\tau = \tau_0$ , for maximum cross-correlation  $R_{1,13}(t_0, \tau)$  of recorded N-S accelerations at channels 1 and 13 (1<sup>st</sup> floor), versus time  $t_0$ , for three earthquakes East of the site (1987 Whittier-Narrows, 1992 Landers and 1992 Big Bear) and one earthquake West of the site (1994 Northridge).

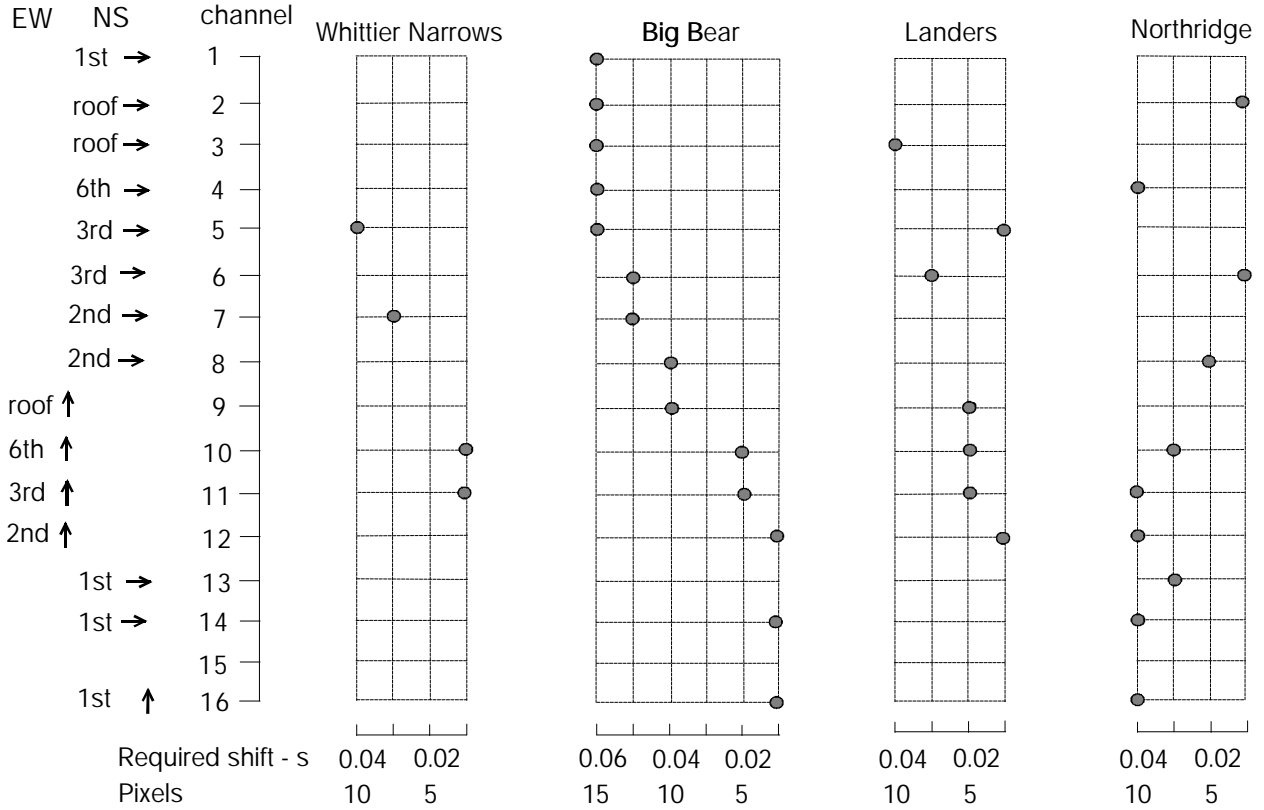


Figure 14 Time shifts for USC digitalization of the CR-1 (channels 1–13) and SMA-1 (channels 14–16) records of four earthquakes, adopted for the analysis of delays in Figures 11–13 (1 pixel ~ 0.004 cm (s)). E.g., shift of 0.04 s means padding four zero-amplitude points (equally spaced at 0.01 s) at the beginning of the record, to delay the recorded motions (i.e. advance the origin time) by 0.04 s.